Industrial Crops & Products 226 (2025) 120649

Contents lists available at ScienceDirect

Industrial Crops & Products

journal homepage: www.elsevier.com/locate/indcrop

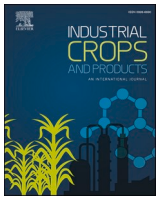

Preparation of high-efficient phosphoric acid modified biochar toward ciprofloxacin removal from wastewater

Ke-Qing Du [a,b], Jun-Feng Li [a], Muhammad Arsalan Farid [a,b], Wen-Huai Wang [a], Guang Yang [a,b,*]

[a] College of Water Conservancy & Architectural Engineering, Shihezi University, Shihezi, Xinjiang 832000, China
[b] Key Laboratory of Cold and Arid Regions Eco-Hydraulic Engineering of Xinjiang Production & Construction Corps, Shihezi, China

ARTICLE INFO

Keywords:
Cotton husk
Biochar
Wastewater
Ciprofloxacin
Adsorption

ABSTRACT

The adsorption of modified biochar can effectively solve antibiotic contamination in water. Nevertheless, few studies have been reported on quantitatively resolving the contribution of each functional group to the adsorption of antibiotics on biochar at the microscopic level, and most modification methods are costly and complex to implement. Therefore, this study successfully synthesized H_3PO_4-modified biochar (PCH) through a one-step process for the removal of ciprofloxacin (CIP) from water. After H_3PO_4 activation, The specific surface area of the PCH rised to 316.1 m^2/g, the pore volume reached 0.45 cm^3/g The Langmuir isothermal model was used to obtain a better match for the adsorption data, the maximum adsorption capacity of biochar at 25°C was 572.8 mg/g, and the adsorption was a self-initiated process of heat absorption. Cotton husk biochar has a higher adsorption capacity compared to commercial activated carbon and biochar prepared from other agricultural precursors, and cost analysis shows that PCH (3.98 $/ kg) is much less expensive than commercial activated carbon (259.5 $/kg). Furthermore, the main mechanisms of CIP adsorption on PCH are pore filling, electrostatic forces, hydrogen bonding and π-π conjugation. Importantly, DFT calculations showed that O-P groups rather than C-P-O groups could serve as the main sites for CIP adsorption. In conclusion, this study provides new insights into the adsorption of antibiotics on phosphoric acid-modified biochar, and it promotes the application of biochar in the remediation of antibiotic wastewater.

1. Introduction

In recent years, pollution of water resources by antibiotic drugs has caused many serious environmental problems. Antibiotics are frequently used in the healthcare and livestock industries (Septian, Shin, 2020). Due to the low level of its utilization by humans and animals, antibiotics have often been discovered in different environmental media, as in sewage, sludge, groundwater, and surface water (Qiao et al., 2018). Ciprofloxacin (CIP) is a third-generation fluoroquinolone antibiotic that is a wide- spectrum antibiotic used to protect against a variety of bacterial infections (Shen et al., 2019). Residual CIP in aquatic environments can be toxic to aquatic plants and animals, even at low concentrations, and the research has found that a concentration range of 50–500 μg/L inhibited DNA topoisomerase (Migliore et al., 2000). Multiple health problems can be induced by CIP in water, including enhanced bacterial resistance, reduced white blood cells, and diarrhea (Shen et al., 2019). Even at low concentrations, CIP may impair lymphocytes, lower sperm counts, and increase the risk of prostate and breast cancer (Lapworth et al., 2012). Studies have shown that CIP concentrations in wastewater from pharmaceutical plants in India have been found to be as high as 31 mg/L (Gani et al., 2017). Thus, it is essential to identify an efficient solution for removing CIP from water to ensure environmental health.

Adsorption (Bello et al., 2019, Khanday et al., 2019), Fenton response (Jiang et al., 2022), oxidation by ozone (Lu et al., 2020), biofilm process (Zhang et al., 2022), photocatalytic degradation (Akter et al., 2022) are common methods in removing CIP. Adsorption is a widely utilized and economically effective technique for removing non-degradable organics from water without generating toxic derivatives (Cheng et al., 2022, Wang et al., 2017). However, other methods can remove CIP to some extent; they have many drawbacks, such as high cost, difficulty in completely eliminating antibiotics, and the possible generation of toxic by-products. Currently, biochar (Khan et al., 2023, Deng et al., 2023), clay minerals (Septian, Shin, 2020),

* Correspondence to: College of Water Conservancy & Architectural Engineering, Shihezi University, Shihezi, Xinjiang 832000, PR China.
E-mail address: mikeyork@163.com (G. Yang).

https://doi.org/10.1016/j.indcrop.2025.120649
Received 30 October 2024; Received in revised form 16 January 2025; Accepted 2 February 2025
Available online 10 February 2025

carbon nanotubes (Oliveira et al., 2023) are frequently used adsorbents for the treatment of antibiotic wastewater. Among these materials, biochar is an economical and eco-friendly option because of its oxygen-containing functional groups resulting from pyrolysis under oxygen-limiting conditions, which can efficiently adsorb pollutants in water (Azzam et al., 2022).

In recent years, China's annual cotton production has surpassed 4 million tons, resulting in a substantial amount of agricultural waste in the form of cotton husk (Wang et al., 2016). Traditional methods of disposing of cotton husks include returning them to the fields or burning them. However, the former method can lead to pest and disease outbreaks in the future because of the high lignin content and dense structure of cotton husks (Zhou et al., 2024). In addition, incineration produces toxic gases that pollute air. Traditional methods of cotton husk disposal not only waste resources but are also harmful to the environment. In cotton production areas, cotton husks are more available compared to biomass feedstocks such as rice straw and straw (Islam et al., 2021, Kwak et al., 2019), which helps to reduce the burden of local agricultural waste. In addition, cotton husk has a higher cellulose content than other agricultural wastes, which is conducive to the preparation of biochar with better physicochemical properties (Kang et al., 2012). Cotton husk accounts for about 27 % of the same plant, and its composition includes 50–72 % cellulose and hemicellulose, which is suitable for the preparation of porous carbon materials (Chen et al., 2022). Unfortunately, to date, studies on the adsorption capacity of biochar extracted from cotton husks for quinolones, such as CIP in water have not been reported.

Many reports have demonstrated that biochar derived from untreated biomass has certain drawbacks. For example, small specific surface area and few numbers and variety of functional groups, which must be addressed to enhance their adsorption properties further. For example, biochar produced using $ZnCl_2$-activated algae has great potential for CIP removal from water (Li et al., 2018). In a sample experiment, the removal rate of 97.92 % was achieved in 120 min using biochar obtained by pyrolysis of N_2 activated bagasse feedstock for adsorption of 30 mg/L CIP (Che et al., 2023). However, these methods are either costly or highly corrosive to containers. Compared with other activators, H_3PO_4 is a green and low-cost chemical activator that can increase the diversity of pore structures during biomass activation (Zhang et al., 2023). Additionally, the introduction of heterogeneous atoms into biochar has an essential effect on the adsorption process, which may disrupt the organized structure of the SP2 carbon network (Ding et al., 2020a). Although previous studies have noted the presence of phosphorus-containing functional groups and confirmed their involvement in the adsorption process, the interactions between functional groups of different configurations and pollutants have not been systematically explored, and the specific contribution of different functional groups to the adsorption of CIP molecules remains unclear (Jiang et al., 2023, Nguyen et al., 2023). Therefore, there is an urgent need to analyze the adsorption behavior of H_3PO_4-modified biochar on CIP from a microscopic perspective and explore the potential effects of P introduction on biochar-pollutant interactions.

In this study, H_3PO_4-modified biochar (PCH) was synthesized from cotton husk by a simple method. The adsorption performance of PCH on CIP was investigated in batch experiments. The main adsorption mechanisms of CIP on PCH were analyzed using adsorption kinetics, isotherms and thermodynamic methods. Additionally, the adaptability of PCH to different conditions and real wastewater was investigated. The present study innovatively introduces DFT calculations based on elucidating the interaction mechanisms of different groups in PCH with CIP molecules through Mulliken charges and indication of surface electrostatic potential (ESP)Furthermore, the economic feasibility of PCH for production applications was evaluated. The results of this study provide a feasible way for the resource utilization of cotton husk in China, and provide a theoretical reference and engineering guidance for the efficient removal of CIP in wastewater.

2. Materials and methods

2.1. Materials

CIP and phosphoric acid (purity ≥99 %) used in this research were purchased from Shanghai MacLin Reagent Company, China. All other chemicals were analytical purity and not processed. Cotton husks were gathered from Xinjiang, China, washed with purified water and dried in a chamber at 60°C. The dried cotton husks were then crushed and passed through an 80-mesh sieve. Deionized water was used to prepare all the solutions.

2.2. Synthesis of adsorbents

In this study, cotton husk powder (10 g) was immersed in 15 mL of 10 %, 20 %, 30 %, and 40 % H_3PO_4 solution, stirred for 15 min, and then pyrolyzed in a tube furnace for 120 min at 300 °C, 400 °C, 500 °C, 600 °C, and 700 °C, respectively. The heating rate of the tube furnace was 5 °C/min, and the N_2 rate was 0.1 L/min. The obtained biochar was then washed several times with deionized water to neutralize and remove excess H_3PO_4. Finally, the material was dried at 80 °C and pulverized to a diameter of less than 0.2 mm, and was labeled as PCH. Biochar that was not activated by H_3PO_4 was obtained by the pyrolysis of 10 g of cotton husk powder by depositing it in a tubular furnace at 600 °C for 120 min. The material was then cleaned, dried, and pulverized using the same methods and labeled as CH.

2.3. Characterization of materials

The materials were characterized using a variety of techniques. The crystal structure of biochar was characterized by X-ray diffractometer (XRD, Shimadzu XRD 7000). The microscopic topography of the materials was obtained by scanning electron microscopy (SEM, Sirion 200). The surface functional groups of the biochar were determined by FTIR (Fourier Transform Infrared Spectrometer, ThermoNicolet Nexus 470) scanning in the wavelength range of 4000–440 cm^{-1}. The pore structures of the materials were characterized using N_2 adsorption-desorption isotherms on a specific surface area analyzer (Micromeritics), and the specific surface areas of the materials were obtained using the BET model. The chemical elemental composition and chemical state of the biochar were analyzed using X-ray photoelectron spectroscopy (XPS, Thermo-VG Scientific)). The pH of nine sets of 100 mL of 0.1 mol/L NaCl sets was regulated from 2 to 10 using 0.01 M HCl and 0.01 M NaOH solutions, and 0.1 g of PCH was added to each set. The final pH was determined after stirring for 24 h, and the zero-charge point of PCH was obtained as the difference between the final pH and the initial pH (pH_{pzc} = final pH - initial pH).

2.4. Adsorption experiments

Batch adsorption experiments of CIP on PCH were performed in 200 mL tapered flasks. The kinetics of the experimental data were obtained by adding 10 mg of PCH to 100 mL of CIP solution at various initial concentrations (30 mg/L, 60 mg/L, 120 mg/L, pH=6), shaken at 120 rpm in a thermostatic shaker, and sampled at different time intervals from 5 to 720 min. Isothermal adsorption experiments were performed by placing 100 mL CIP solution (initial concentrations ranged from 20 to 160 mg/L, pH = 6) containing 10 mg/L PCH at 15 °C, 25 °C, and 35°C with shaking for 12 h. The influence of pH on CIP adsorption by PCH was analyzed by adjusting the pH in the range of 2–10. The adsorption behavior of PCH containing 25 mM, 50 mM, and 100 mM of coexisting ions was tested at the same CIP concentration, respectively. At the time of sampling, 2 mL of the mixture was drawn and centrifuged at 3000 rpm to separate the adsorbent from the liquid, which was then filtered through a 0.45 μm filter membrane. The concentration of residual CIP in the filtrate was detected using a UV-Vis spectrophotometer

(Cary 4000, Agilent, USA) at a maximum absorption wavelength of 277 nm. Each set of experiments was repeated thrice, and the mean values were calculated. All the models and equations used in this study are available in the Table S1. The molecular structure optimization and wave function analysis of CIP and PCH were calculated by Gaussian 16 program with B3LYP/6–31 G* , and the interactions could be corrected by B3LYP-D3 (Ding et al., 2020b).

3. Results and discussions

3.1. Optimization of biochar preparation

The synthesis conditions of biochar are crucial factors that influence its adsorption performance. In this study, biochar synthesized using different volume fractions of H_3PO_4 impregnation and different carbonization temperatures were screened, and the optimal conditions were selected for subsequent experiments, and the results are shown in Fig. 1. At all carbonization temperatures, the adsorption capacity of PCHs for CIP almost always showed an increasing and then decreasing trend with the increase of H_3PO_4 volume fraction. This is due to the fact that sufficient amount of H_3PO_4 interacts with the lignin in the biomass and breaks the low energy base bonds (e.g., α-O-4). The breaking of these bonds generates small molecules which gradually volatilize at high temperatures, thus providing more adsorption sites for the char material. However, an excessively high concentration of H_3PO_4 can lead to pore structure fragmentation. In addition, the carbonization temperature had a significant effect on the adsorption performance of the material. PCH showed better adsorption effect at 600℃. With the carbonization temperature increased, the pore structure inside the biochar was expanded. However, when the temperature was further increased, the functional groups might disappear due to the increase of graphitization, which weakened its adsorption capacity (Angin, 2013). Based on the preliminary screening and study results, PCH with the volume concentration of 30 % and the carbonization temperature of 600℃ was selected as the best adsorbent for further studies.

3.2. Characterization of materials

In Fig. 2a and b, SEM images show the microscopic morphology of the biochar before and after modification. Compared with CH, the particle distribution on the surface of PCH was more homogenized, implying that the pores of the H_3PO_4-activated biochar were well developed. Fig. 2c shows the XRD patterns of CH and PCH. The low

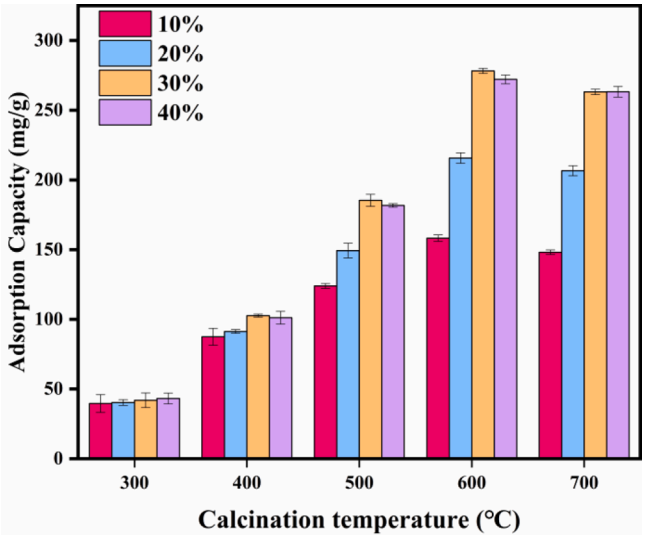

Fig. 1. Adsorption performance of the biochar produced under different preparation conditions.

degree of crystallization of the virgin biochar indicates the ease of the modification reactions. The peaks observed at approximately 2θ= 26° and 44°for both biochar corresponded to the (002) and (101) facets, suggesting that pyrolysis and acid activation processes promote the formation of graphitic structures (Wang et al., 2017). Apparently, H_3PO_4-activation significantly enhanced the graphitization of PCH, and ensured a high π-electron cloud density that facilitates π-π interactions with CIP.

The FTIR spectra of PCH and CH in the Wavelength band of 4000–440 cm^{-1} were used to study the surface functional groups of the materials (Fig. 2d). The wide absorption peak of both materials found at 3430 cm^{-1} is ascribed to the O-H stretching vibrations of lignin and cellulose (Qu et al., 2020). Furthermore, the peak at around 1580 cm^{-1} is responsible for the C═C stretching of aldehydes, ketones, or esters in both materials suggests the formation of aromatic structures in the biochar (Zhang et al., 2023). This improvement in aromaticity was beneficial for enhancing the hydrophobicity of the materials and further increasing their adsorption of antibiotics. H_3PO_4-activated biochar eliminated the vibration peaks associated with -CH_2 stretching (Li et al., 2019). However, the pyrolysis of PCH generated new peaks at 1164 cm^{-1} and 493 cm^{-1} corresponding to the O-P and C-P-O groups, respectively, proving that the phosphate group was successfully grafted onto the surface of the biochar (Liu et al., 2021).

The adsorption-desorption curves and pore size distributions of the prepared cotton husk biochar are shown in Fig. 3a and b. It can be observed that within the relative pressure range of 0.45–0.9, CH exhibited type II isotherms and H3 hysteresis loops, while PCH demonstrated type IV isotherms and H4 hysteresis loops. The pore-size distribution curves showed that PCH and CH were characterized by typical mesoporous structures (2–50 nm). In Table S2, PCH exhibited a higher specific surface area (316.1 m^2/g) than CH, which is favorable for the elimination of pollutants. The total pore volume of PCH was enhanced from 0.19 cm^3/g to 0.45 cm^3/g compared to CH, which may be attributed to the inhibition of carbon skeleton collapse and fragmentation by H_3PO_4 during pyrolysis, thus enhancing the pore volume of the biochar (Liu et al., 2021). The numbers of S_{mic} and S_{mes} nearly doubled, indicating the presence of a distinct hierarchical pore structure. These results suggest that H_3PO_4 activation is conducive to improving the pore volume and specific surface area of biochar.

The XPS spectra of C1s, O1s, and P2p for biochar before and after modification were deconvoluted and fitted using Advantage software (Fig. 3c). In Fig. 3d, the deconvolutional peaks of CH at 284.8 eV, 286.5 eV, 288.7 eV, and PCH at 284.8 eV, 286.2 eV and 290.1 eV were attributed to C-C, C-O, O═C/C-P bonds (Akhavan, 2015), respectively. After modification, the proportions of C-O and O═C/C-P significantly increased (Fig. 3d), which is consistent with the literature (Peng et al., 2017). The proportion of C-C(59.4 %) bonds is relatively high, indicating a high degree of graphitization in the sample. In Fig. 3e, the two peaks 531.4 eV and 533.2 eV of the O1s spectrum of CH are attributed to -OH and O-N. Whereas the peaks of the O1s spectrum of PCH located at 533.1 eV, 531.3 eV, and 536.7 eV are related to O-P, C-O, and chemisorbed O, respectively. This result indicates that H_3PO_4 activation changed the chemical valence of oxygen. The P2p peaks were observed in the full spectrograms, and the sites with binding energies of 133.6 eV and 133.2 eV after peak splitting were attributed to the O-P and C-P-O groups (Fig. 3f), respectively (Guo and Rockstraw, 2007). As a result, phosphorus forms phosphoric acid functional groups on the PCH surface in a phosphate-like structure, which are strongly polarized and readily combine with the carboxylic acid groups on the CIP molecule through hydrogen bonding.

Based on the above characterization results, the improved adsorption performance of PCH can be mainly attributed to the significant developmental grading of the pores and the increase of phosphate functional groups. Phosphoric acid activation facilitated the formation of micro- and mesoporous structures during the pyrolysis of cotton husks, which in turn improved the specific surface area of the adsorbent and

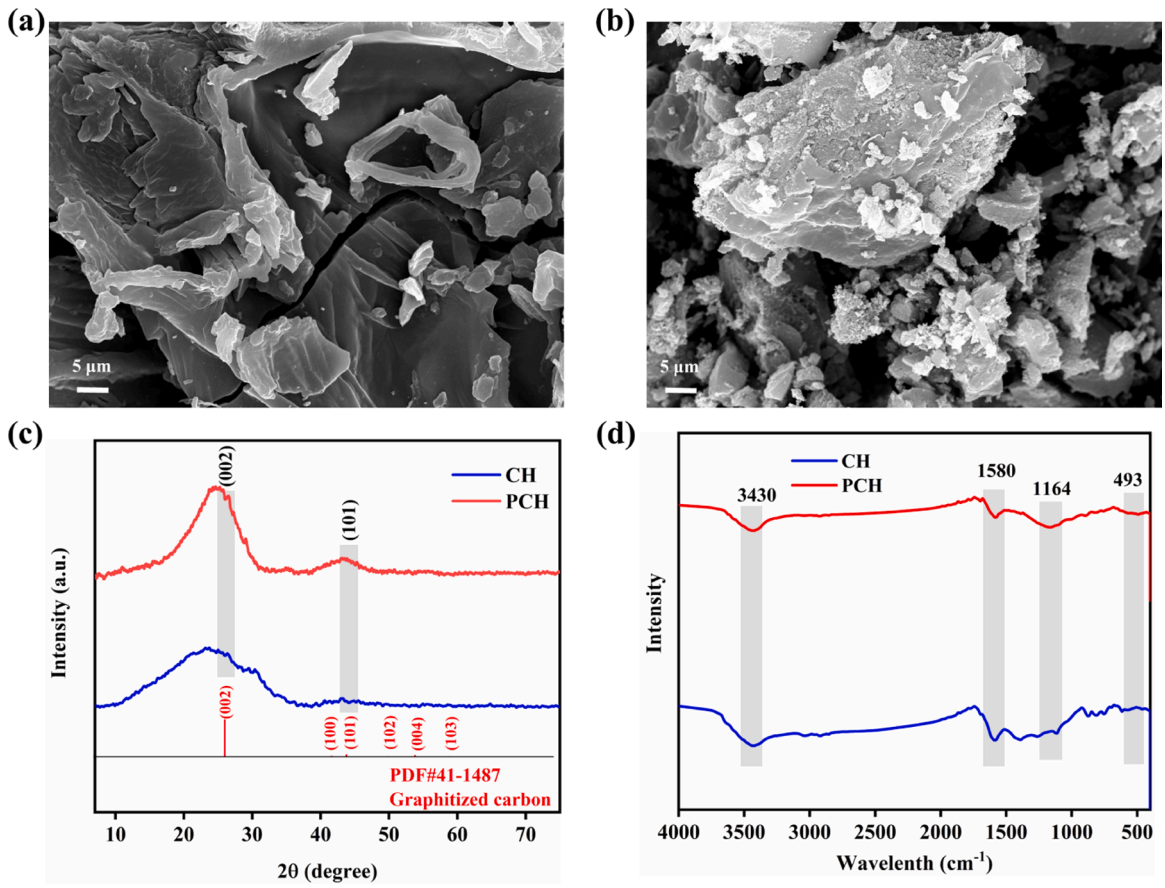

Fig. 2. SEM images of (a) CH and (b) PCH, (c) XRD patterns of PCH and CH, (d) FTIR spectra of PCH and CH.

generated additional active sites for CIP removal. The increase in the phosphorus-oxygen functional groups enhanced the polarity of PCH, thereby promoting its binding to the polar molecule CIP. The following experimental results verified these inferences.

3.3. Adsorption performance

3.3.1. Contact time and adsorption kinetics

The variation in the CIP removal rate with contact time (5–720 min) at different primary concentrations is shown in Fig. 4a, the CIP adsorption amount rise rapidly in the first hour, and as time went by, the rate of CIP adsorption decreases gradually due to mutual repulsion of CIP molecules adsorbed on the surface of the adsorbent and CIP molecules in solution as well as saturation of the active sites (Fries et al., 2016). It can be found that adsorption balance was reached in about 4 h regardless of the initial concentration of CIP.

In this research, the adsorption kinetics of CIP on PCH at various initial concentrations were studied by using the proposed first-order and second-order models. As shown in Table 1, the results of the experimental data were more consistent with the pseudo-second-order model. (R^2=0.997–0.999). Moreover, the adsorption capacities computed by the pseudo second-order model for CIP with preliminary concentrations of 30 mg/L, 60 mg/L and 120 mg/L are 279.2 mg/g, 407.2 mg/g and 592.2 mg/g, which are closer to the experimental results (281.4 mg/g, 410.4 mg/g, 599.8 mg/g). These results indicated that the chemical behavior was the main factor controlling CIP sorption on PCH (Fries et al., 2016). Hence, the ideal adsorption capacity and short adsorption cycle of PCH can effectively reduce the investment costs in practical applications.

To further explore the adsorption mechanisms, the experimental results were fitted segmentally by intra-particle diffusion model. As shown in Fig. 4b and Table 2, the high R^2 values of the fitted curve indicate high credibility of the fitting. The adsorption behavior of PCH on CIP was separated into three main phases: film diffusion, inter-particular diffusion, and solute adsorption. The adsorption rate decreased sequentially in all three phases, which implies a gradual increase of the diffusion layer thickness and diffusion resistance as the sorption sites on the PCH surface are filled with CIP molecules (Zhang et al., 2021). Moreover, the fitted curves did not cross the point of origin, indicating that inter-particle diffusion was not the exclusive controlling factor in the sorption of CIP by PCH, and was also affected by film diffusion.

3.3.2. Influence of initial pH

The initial pH of the solution is considered to be a critical influence on the apparent properties of the adsorbent and the form in which the adsorbate dissociates (Li et al., 2014). Fig. 4c shows the change in the adsorption capacity at pH values in the range of 2–11, with a gradual increase in the adsorption capacity of CIP onto PCH as the pH increased from 3 to 6. The maximum adsorption capacity reaches 295.2 mg/g at pH 6. As the pH increases from 8 to 11, the adsorption capacity of PCH rapidly decreased. Similar trends have also been reported in the literature (Septian, Shin, 2020). The pK_{a1} and pK_{a2} of CIP are 6.25 and 8.78, respectively. CIP hydrolyzes to a cation when pH < 6.05 but to an anion at pH > 8.78 and is electro-neutral in the range of pH 6.25–8.78 (Sun et al., 2016). Moreover, the pH_{pzc} of PCH was 2.57 (Fig. 4c), indicating the presence of strongly acidic groups. When pH > pH_{pzc} , the PCH was negatively charged, whereas it was positively charged when pH < pH_{pzc} (Gadekar et al., 2020). Consequently, at a low pH, the adsorption capacity of PCH is reduced owing to CIP protonation in acidic solutions, where excess H^+ competes with CIP for adsorption sites. However, when the solution pH exceeded 2.57, PCH was negatively charged and

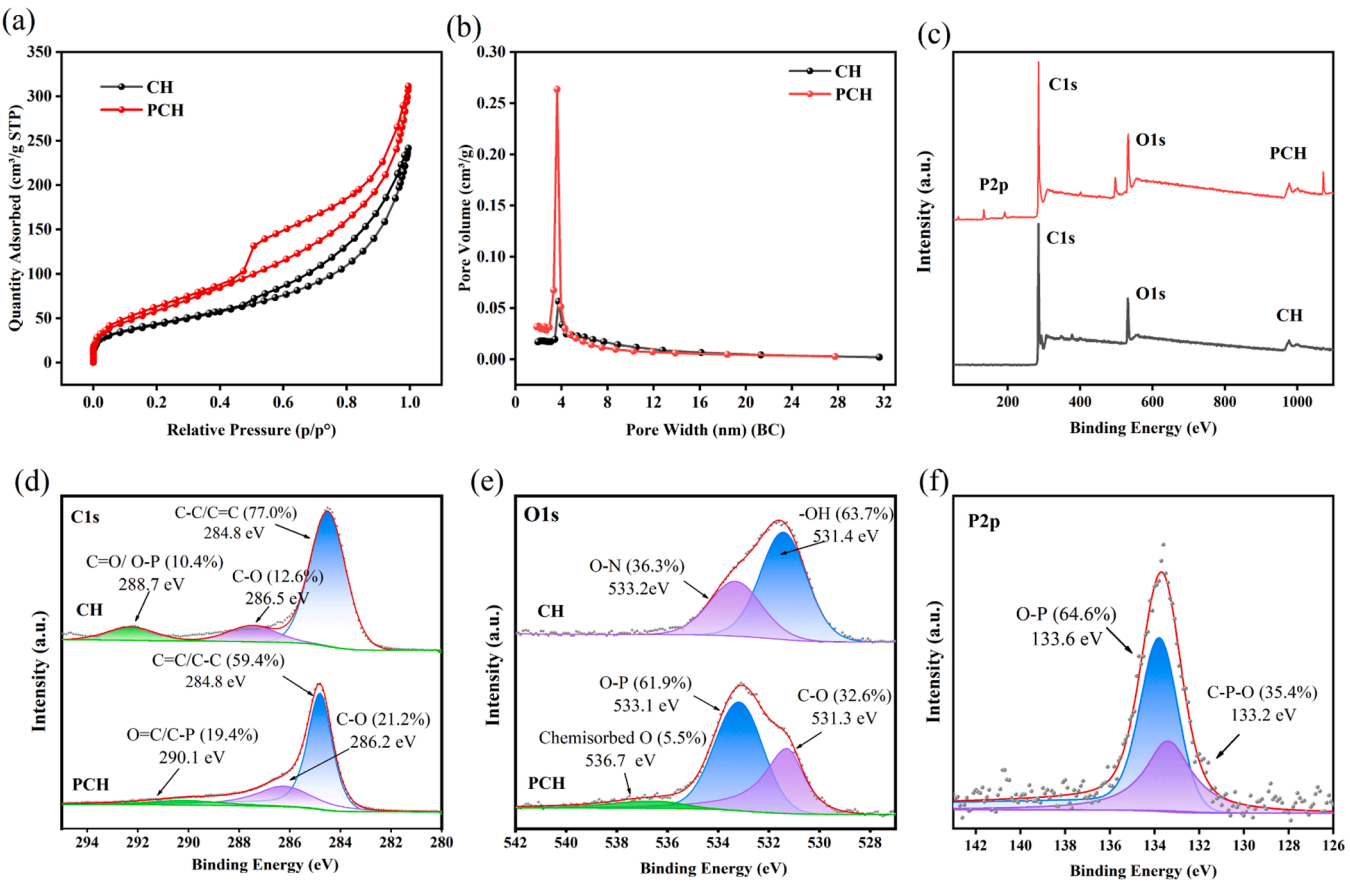

Fig. 3. (a) Nitrogen adsorption–desorption isotherms of CH and PCH, (b) pore size distribution curves of CH and PCH, (c) Full-scale XPS spectrum of CH and PCH, (d) C1s pectrum of CH and PCH, (e) O1s pectrum of CH and PCH, and (f) P2p spectrum of PCH.

exhibited a strong electrostatic adsorption effect on CIP in its cationic form. Under alkaline conditions, the abundant OH^- in the solution hindered the sorption of CIP onto the adversely charged PCH surface.

3.3.3. *Influence of coexisting ions*

Fig. 4d shows that CIP adsorption was affected by different ionic intensities. The presence of Na^+, K^+, NO^{3-}, and SO_4^{2-} had negligible effects on the CIP adsorption. However, a slight decrease of CIP adsorption concentration might be attributed to the "squeezing out" effect when these ions concentrations were rising (Carabineiro et al., 2011). In addition, the existence of Ca^{2+} and Mg^{2+} had a hindering impact on CIP adsorption, and the adsorption amount was reduced by approximately 12 % compared with that of the control group with pure water as the background solution. The inhibitory influence was more significant when the concentration of Mg^{2+} and Ca^{2+} was higher because of the larger hydration radius of divalent cations, which exhibited stronger competitiveness in adsorption sites compared to CIP on the surface of biochar (Alver et al., 2020). It could be seen that CO_3^{2-} had a notable inhibitory impact on the adsorption of CIP, and the adsorption amount of PCH was reduced by 17.8 %, 22.7 %, 25.9 % in the existence of three various concentrations of CO_3^{2-}, respectively. This phenomenon was caused by the squeezing action of CO_3^{2-} on the biochar, causing the aggregation of biochar particles, thereby reducing the number of available sites. In addition, the extrusion effect leads to disruption and clogging of the pore structure of biochar. These results indicate that PCH can also exhibit favorable adsorption characteristics in the presence of competitive ions.

3.3.4. *Influence of adsorbent dose*

The use of optimum dosage of carbon material is required for cost-effective removal of CIP from water. As shown in Fig. 5a, the removal of CIP was significantly increased to 94.17 % when the PCH dosage was increased from 0.05 g/L to 0.1 g/L at an initial concentration of 30 mg/L. At similar concentrations previously reported, other literature reported only 85.30 % and 89.94 % CIP removal (Xue et al., 2022, Hamadeen and Elkhatib, 2022). This is attributed to the increased number of active sites and surface area (316.7 m^2/g) provided by the PCH material, as well as the driving force generated by the antibiotic concentration gradient between the adsorbent and the solution (Roy et al., 2022a). In addition, CIP was able to form hydrogen bonds with the abundant phosphorus-oxygen functional groups on the PCH surface, which is consistent with the XPS characterization results. When the PCH dosage was further increased from 0.1 g/L to 0.2 g/L, the removal rate only increased by about 5.4 %. Meanwhile, the equilibrium adsorption capacity decreased rapidly from 282 mg/g to 149 mg/g. Therefore, the highest removal rate and adsorption capacity were achieved when the PCH dosage was 0.1 g/L.

3.3.5. *Influence of adsorption temperature*

The effects of solution temperature (288 K, 298 K, 308 K) on the adsorption experiments are shown in Fig. 4b. When the initial concentration of CIP was greater than 30 mg/L, the equilibrium adsorption of PCH at the same initial concentration increased significantly with increasing temperature, which may be caused by the enhancement of the number of adsorption sites and diffusive mobility owing to the increase in temperature (Ghasemi, Asadpour, 2007). It indicates that higher temperature facilitates adsorption,and the adsorption process is a heat-absorbing reaction.

The adsorption isotherms were derived by fitting the experimental results using the Langmuir, Freundlich, and Temkin equations (Fig. 5c-

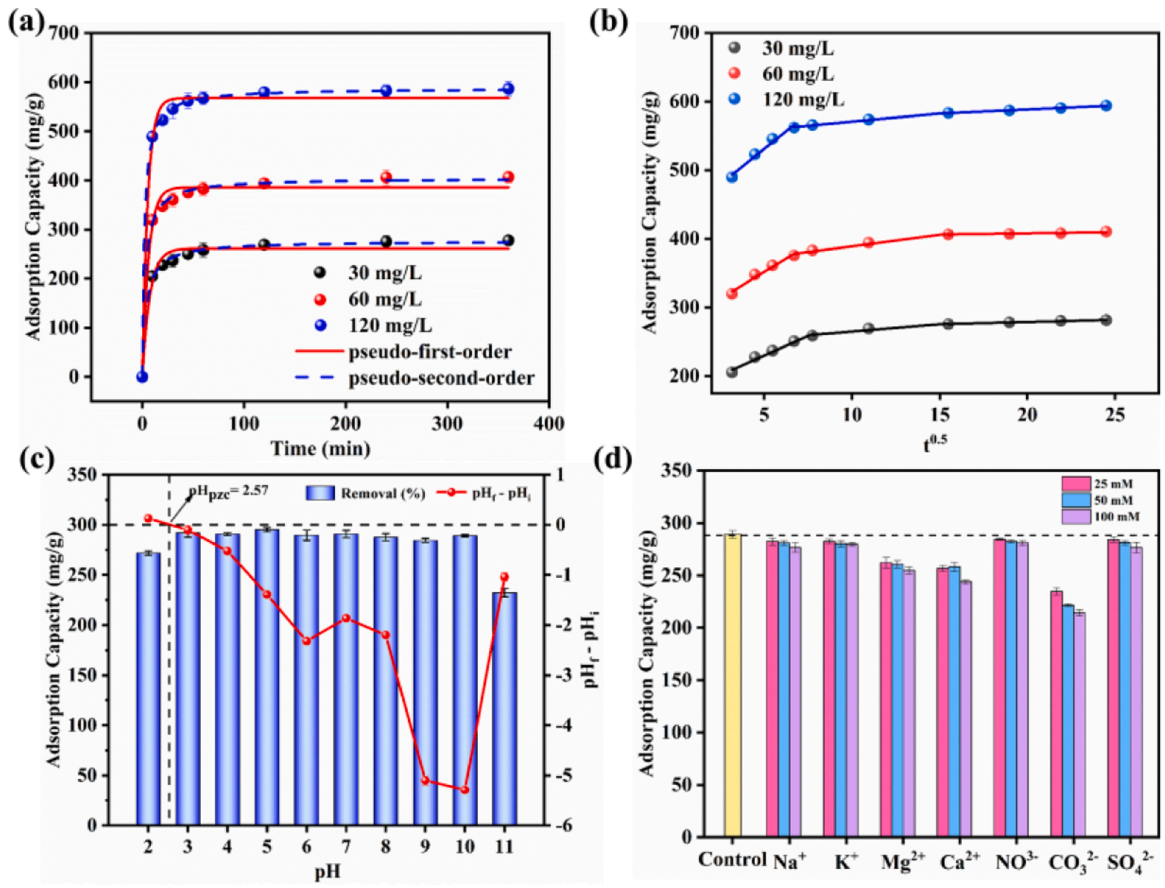

Fig. 4. (a) Adsorption kinetics of CIP onto PCH by pseudo-first-order and pseudo-second-order models, (b) Intra-particle diffusion model, (c) The influence of pH on CIP adsorption and pHpzc of PCH, (d) Influence of coexisting ions (C_0=30–120 mg/L,adsorbent dosage =0.1 g/L, the reaction time =6 h, pH=6, at 15, 25, 35℃).

Table 1
The kinetic datas for CIP adsorption onto PCH.

C_0	Pseudo- first-order model			Pseudo- second-order model			Q_m^{exp}
(mg/L)	k_1 (1/min)	Q_m^{theo} (mg/g)	R^2	k_2 (1/min)	Q_m^{theo} (mg/g)	R^2	(mg/g)
30	0.1222	267.1	0.970	0.00085	279.2	0.997	281.4
60	0.1492	392.4	0.979	0.00079	407.2	0.998	410.4
120	0.2040	583.9	0.901	0.00073	592.2	0.999	599.8

e), this was performed to investigate how the solute was distributed on the surface of PCH in the solution when adsorption equilibrium was reached. Table 3 shows that the Langmuir model achieves the best fit to the experimental data, and the theoretical adsorption capacities computed using the Langmuir model were more similar to the experimental results. This implies that the adsorption of CIP on PCH was monolayer adsorption associated with chemisorption (Kunwar et al., 2015). The Freundlich model also fit the data well, with 1/n values less than 1, indicating multilayer adsorption and affinity adsorption for PCH in the CIP adsorption process. The Temkin model had a good linear relationship ($R^2 > 0.977$), which also indicates that the adsorption process involving chemisorption and adsorption decreased linearly with surface coverage (Zhou et al., 2018). Table 4 shows the CIP adsorption amount of PCH compared with those of previously reported adsorbents, indicating the excellent adsorption performance of PCH.

3.3.6. *Adsorption thermodynamics*

The thermodynamic data are summarized in Table S3. The results showed that $\Delta G < 0$ at various temperatures, implying that the adsorption of CIP on PCH was spontaneous. As the temperature increases, a more negative ΔG value is observed, indicating that adsorption is more likely to occur. The results of $\Delta H > 0$ means that the adsorption involves a heat-absorbing reaction (Yahiat et al., 2011). The positive value of ΔS implies that the adsorption course is unreversible and that the solid-liquid interface is very irregular (Wei et al., 2013).

3.4. *Economic assessment*

The economic assessment of PCH is crucial in specific applications. The cost of treating wastewater by PCH depends mainly on the consumption of materials, energy and labor. Detailed information on treatment costs is shown in Table S4. Nevertheless, the preparation cost

Table 2
The intraparticle diffusion kinetic datas for CIP adsorption on PCH.

C_0	film diffusion			inter-particular diffusion			solute adsorption		
(mg/L)	k_1	C_1	R^2	k_2	C_2	R^2	k_3	C_3	R^2
30	11.4	172.7	0.978	2.1	243.4	0.971	0.7	265.5	0.990
60	15.6	273.8	0.976	3.3	355.6	0.975	0.4	400.8	0.997
120	20.6	427.9	0.979	2.4	546.8	0.994	1.2	564.8	0.996

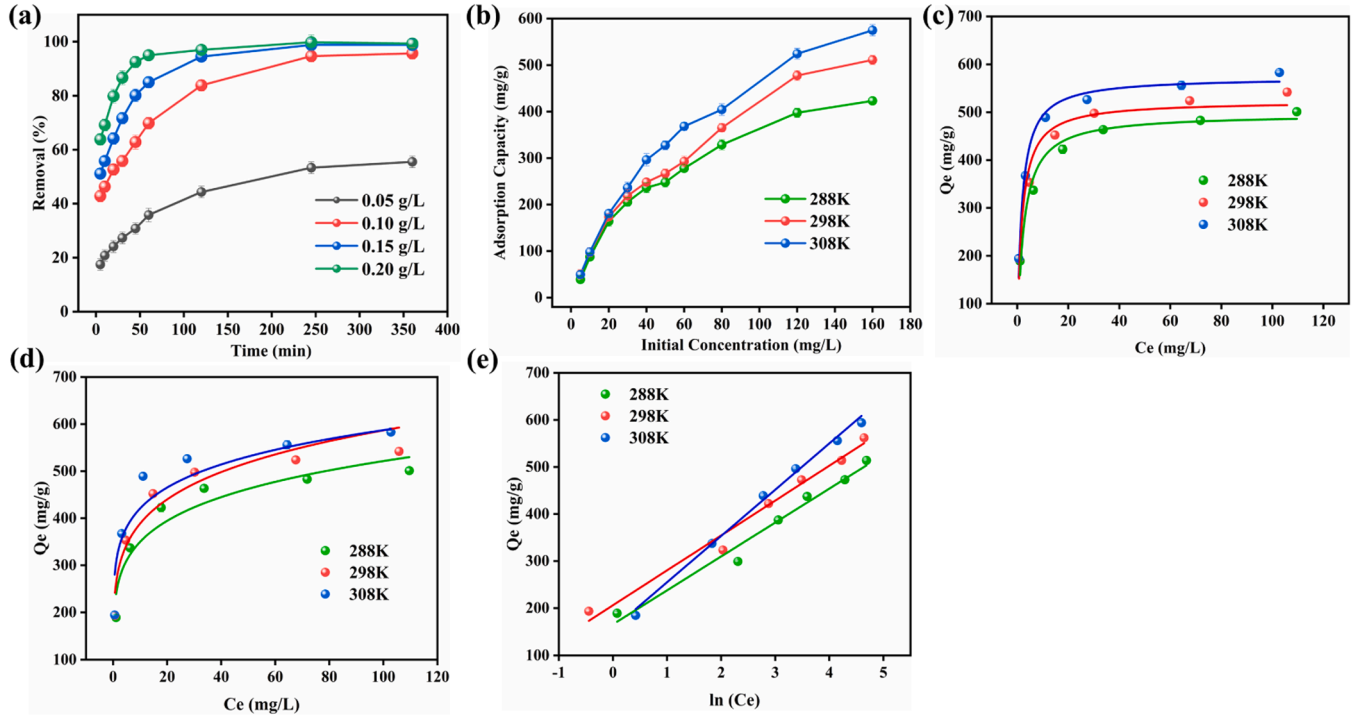

Fig. 5. (a) Influence of adsorbent dose, (b) Influence of adsorption temperature, Adsorption isotherms simulated with (c) Langmuir, (d) Freundlich and (e) Temkin models.(C_0=30–120 mg/L, adsorbent dosage =0.1 g/L, the reaction time =6 h, pH=6, at 15, 25, 35℃).

Table 3
The isotherm datas for CIP adsorption on biochar.

T * (K)	Q_m^{exp} (mg/g)	Langmuir			Freundlich			Temkin		
		Q_m^{theo} (mg/g)	K_L (L/mg)	R^2	K_F (mg/g)	1/n	R^2	K_T (L/g)	b_T (J/mol)	R^2
288	524.1	496.4	0.43	0.973	234.7	0.17	0.918	19.4	35.1	0.969
298	572.8	523.0	0.58	0.957	257.7	0.14	0.928	24.4	33.8	0.979
308	621.4	572.8	0.61	0.982	301.7	0.14	0.900	62.6	38.1	0.950

Table 4
Comparison of adsorption amounts of various carbon-based adsorbents for CIP reported in the previous publications.

Material	S_{BET} (m^2/g)	T (℃)	Q_e (mg/g)	Refs.
Biochar (Chitin)	1199	50	245.1	(Khanday et al., 2019)
Commercial activated carbon	644	30	13.6	(Penafiel et al., 2021)
Biochar (Used tea leaves)	8.06	40	238.1	(Li et al., 2018)
Biochar (Camphor leaves)	915	40	449	(Hu et al., 2019)
Biochar (Sewage sludge)	47.5	35	62.4	(Li et al., 2022)
Biochar (Sugarcane bagasse)	1712.2	30	212	(Che et al., 2023)
Biochar (brown algal)	1326	35	434.8	(Nguyen et al., 2022)
Biochar (banana peel)	456.04	30	41.66	(Azzam et al., 2022)
Biochar (grapefruit peel)	/	20	154.89	(Afzal et al., 2019)
Biochar (pomegranate peel)	1149.62	25	142.86	(Hamadeen and Elkhatib, 2022)
Biochar (Cotton husk)	316.1	25	572.8	**This work**

of biochar synthesized from activated sludge was 19 $/kg (Martínez-Alvarenga et al., 2024).The cost of activated carbon prepared from soybean hulls was 42.5 $/kg (Ng et al., 2003).PCH is cheaper compared to commercial activated charcoal (259.5 $) (Bello et al., 2019). In addition, the level of adsorption of CIP by the biochar prepared in this study (572.8 mg/g) was higher than that of other recorded adsorbents. Therefore, the expected cost of treating 1 kg of CIP is 7.64 $, while other activated carbons for CIP removal would be more expensive. This indicates that cotton husk feedstock has the potential to be utilized in large-scale production.

3.5. Adsorption mechanisms

The fluorine atom attached to the benzene ring in the CIP molecule exhibited intense electron-withdrawing ability, resulting in the electron-deficient benzene ring being equivalent to a π-electron recipient. Concurrently, the -OH units on the surface of the adsorbent can function as a π-electron donor, enabling the formation of π–π EDA interactions between them (Alver et al., 2020). This interaction can account for the sorption of CIP by PCH. Furthermore, -NH group in the CIP molecule could interact with the abundant -OH and -COOH groups on the PCH surface through H-bonding. Under the experimental pH conditions, CIP existed mainly as a cation, whereas at pH > pH_{pzc} (2.57), PCH became negatively charged (Che et al., 2023). Thus, electrostatic interactions also have a prominent effect in the adsorption course. The BET results (Table S2 and Fig. 6a and b) showed that H_3PO_4 activation introduced abundant microporous and mesoporous structures to the biochar, indicating that the pore formation was graded with an average pore size of 8.2 nm, which allows for the easy migration of CIP molecules

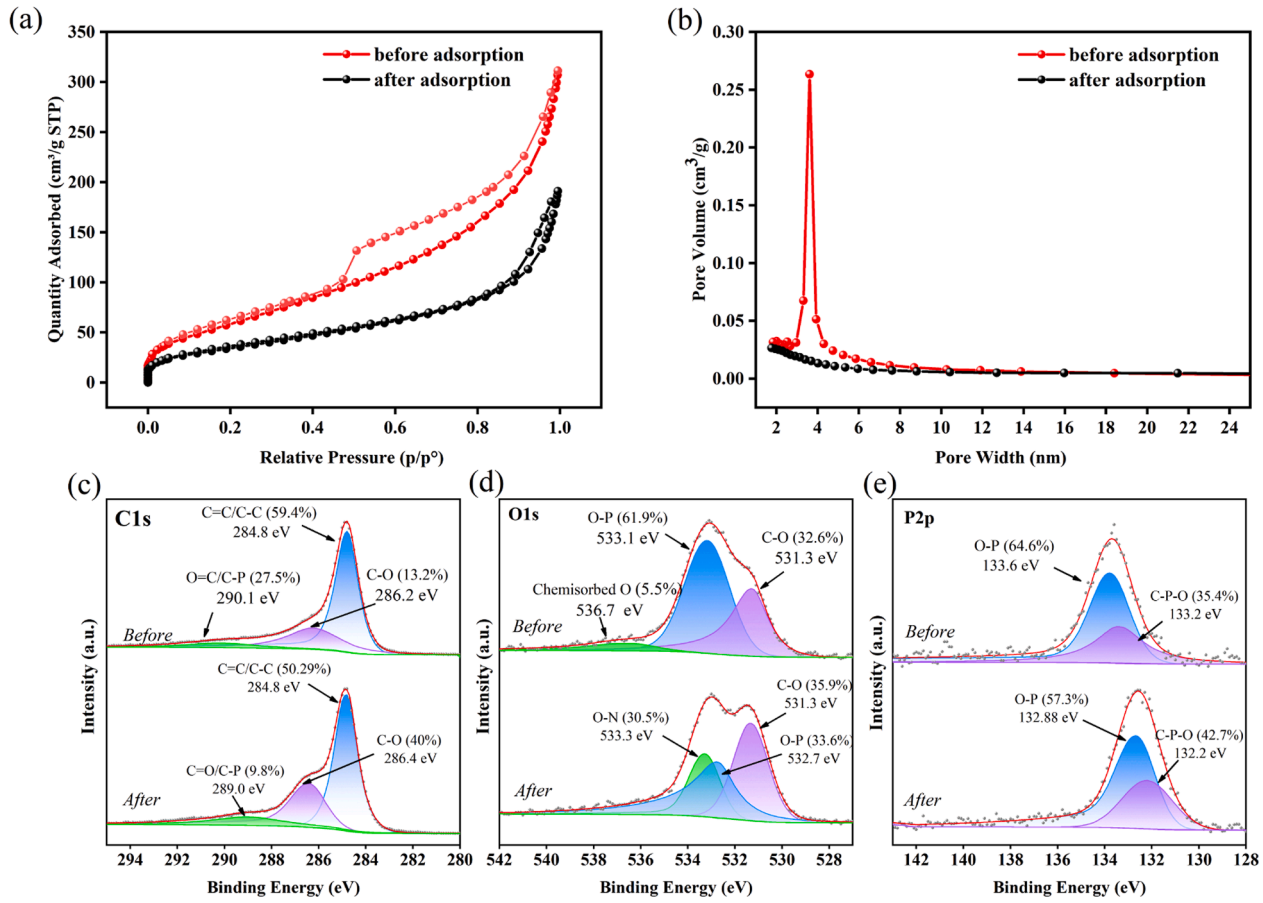

Fig. 6. (a) Nitrogen adsorption isotherms and (b) pore size distributions of PCH before and after adsorption, (c-e) high-resolution XPS spectra of PCH before and after CIP adsorption.

(0.8–1.22 nm in diameter) into the interior of the adsorbent through pore filling. According to the XPS spectroscopic detection (Fig. 6c), there was no significant difference in the C1s spectrum of PCH before and after adsorption.Nevertheless, the increase in the area of the C-O and C═O/C-P peaks suggests that chemisorption may have occurred between the CIP and the oxygen-containing groups on the adsorbent (Fig. 6c). In the O1s spectra after adsorption (Fig. 6d), the deconvolution peaks located at 531.3 eV, 532.7 eV, and 533.3 eV corresponded to C-O, O-P, and O-N, respectively. The O-N peaks were attributed to the binding of the -NH bond in CIP to the O-P bond in PCH (Jiang et al., 2023). Addictionally, the characteristic P2p peak shifted to 132.8 eV and 132.2 eV towards a low bingding energy (Fig. 6e), this indicated that the strongly polar phosphorus-containing groups may bind to the CIP through hydrogen bonding (Liu et al., 2021).

To further elucidate the role of each functional group, the surface electrostatic potential (ESP) distributions and Mulliken charges of CIP and PCH were analyzed. As shown in Fig. 7, the red and blue regions indicated areas of high and low electron density on the surfaces of CIP and PCH, respectively.The electronegativities of oxygen, nitrogen, carbon, and hydrogen are 3.44, 3.04, 2.55, and 2.20 (Cheng et al., 2022), respectively. Atoms with higher electronegativity have a greater ability to attract electrons (Deng et al., 2023, Roy et al., 2022b). Therefore, the oxygen and nitrogen atoms in -OH and -NH groups have stronger electron-withdrawing abilities compared to the adjacent carbon atoms. This enhances the partial positive charge on the hydrogen atoms in -OH and -NH groups, resulting in higher electrostatic potentials on the surrounding surfaces. Consequently, these regions become more susceptible to nucleophilic reactions. Obviously, the N-containing functional group enriched the electron density of CIP (Fig. 7a), which facilitated the complexation of CIP with PCH through the π-bonding of the aromatic ring to form a conjugated system. Upon modification of graphite plane, PCH with -OH, C═O, O-P and C-P-O groups (Fig. 7b-f), the overall potential of the aromatic ring increased. However, the potential at the edges of the functional groups decreased significantly, particularly for the O-P group. These results suggest that CIP is more likely to interact with these functional groups of PCH (Zhang et al., 2022). The Mulliken charge values are shown in Table S5. Hydrogen is the least electronegative in the CIP molecule and is more likely to be positively charged in the molecule. Therefore, the oxygen atoms from the -OH (O41), C═O (O40), O-P (O37), and C-P-O (O39) groups displayed significantly stronger binding to the donor (H38) of CIP compared to other hydrogen bond acceptors. Similarly, O34 of CIP is capable of binding to the donor (H42) of the C-P-O group. The adsorption energy calculations is shown in Table S6, revealing the absolute values of the adsorption energies of various functional groups to CIP: E_{ad} (O-P) = -1.113 eV > E_{ad} (C-P-O) = -0.635 eV > E_{ad} (C═O) = -0.425 eV > E_{ad} (-OH) = -0.327 eV > E_{ad} (CH) = -0.261 eV. The ESP and adsorption energy results mutually support the conclusion that the O-P structure of PCH may contribute most to CIP removal through hydrogen bonding interactions.

3.6. Reusability of PCH for CIP adsorption

The recycling performance of the adsorbents is of great significance for practical applications. To evaluate the regeneration ability of PCH, EtOH and 2 M HCl, 2 M NaOH were used as desorption agents for biochar regeneration (Fig. 8a). The findings disclosed that the adsorption capacities after three cycles were 150.33 mg/g, 156.49 mg/g, and 196.96 mg/g, respectively, which accounted for 54.04 %, 56.25 %, and 70.79 % of the control group's adsorption capacities. The adsorption capacity of PCH significantly decreased after 3 cycles, when 2 M HCl and

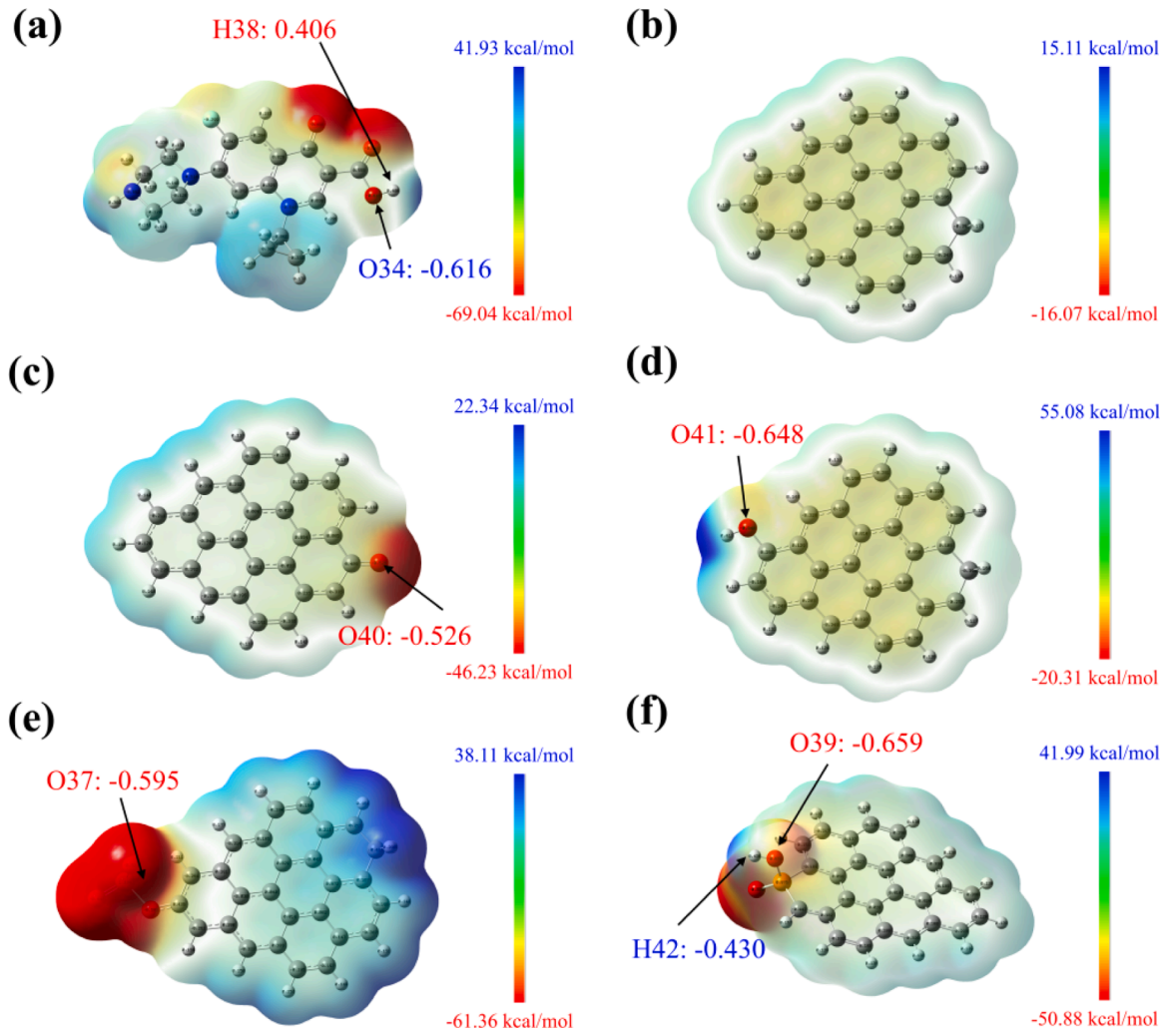

Fig. 7. The surface ESP and Mulliken charge distributions of (a) CIP, (b) CH and (c-f) PCH wtih different oxygen-containing functional groups.

2 M NaOH were added compared to the addition of EtOH. This indicates that the desorption effects of HCl and NaOH on CIP are undesirable. However, this result indicates that PCH exhibits relatively good adsorption stability in acidic and alkaline environments. When EtOH was used as the desorption agent, PCH was capable of effectively removing CIP in each cycle, and it retained a good adsorption capacity after 3-cycles. These results indicate that PCH exhibited excellent recyclability.

3.7. Application of PCH in realistic wastewater and other organic pollutant

Pharmaceutical wastewater (secondary effluent) was used to estimate the performance of PCH in eliminating pollutants from the real wastewater. Added 1 g/L of PCH to the wastewater without pH adjustment, and the mixture was then stirred at 120 rpm for 2 h. Three-dimensional excitation emission matrix fluorescence spectroscopy (3D EEMs) showed strong peak (E_x/E_m of 220–400 nm/330–520 nm) of the original pharmaceutical wastewater indicated the presence of multiple pollutants, and the fluorescence intensity disappeared after adsorption (Fig. 8b and c), implying that PCH had a significant impact on real wastewater. In addition, COD_{Cr} (mg/L) was detected to decrease from 486.45 to 50.14, and TOC (mg/L) was measured to have decreased from 71.63 to 21.33, which satisfied the emission standards of 120 mg/L and 30 mg/L (SEPA, 2008), respectively. PCH also reduced the color of the effluent, transforming it from brown to transparent (Fig. S1). These results further suggest that PCH has great potential for application in wastewater purification.

To further test the adsorption performance of PCH, its ability to remove other types of contaminants, such as orange-yellow G (OG), tetracycline (TC), and acetaminophen (AP), was tested. As shown in Fig. 8d-f, for any pollutant with a concentration of less than 40 mg/L, the elimination rate will be at least 85 %. The results show that PCH exhibits commendable universal performance in practical applications.

4. Conclusion

In this work, PCH was successfully synthesized by activating cotton husks with H_3PO_4 and applied for adsorption of CIP. H_3PO_4 activation improved the pore volume (0.45 cm^3/g) and specific surface area (316.1 m^2/g) of the biochar. The largest adsorption capacity of PCH for CIP amounted to 572.8 mg/g at 25℃, which is attributed to the plentiful functional groups and ideal pore structure of PCH. The economic assessment indicates that the production PCH are highly feasible. DFT calculations demonstrates that the O-P group has the highest adsorption energy for CIP. Combined with the ESP results, it indicates that the O-P structure may significantly contribute to the removal of CIP through hydrogen bonding. Moreover, PCH has superior adsorption characteristics for real wastewater and various organic pollutants. Thus, PCH may be a prospective material for the elimination of organic contaminants from wastewater.

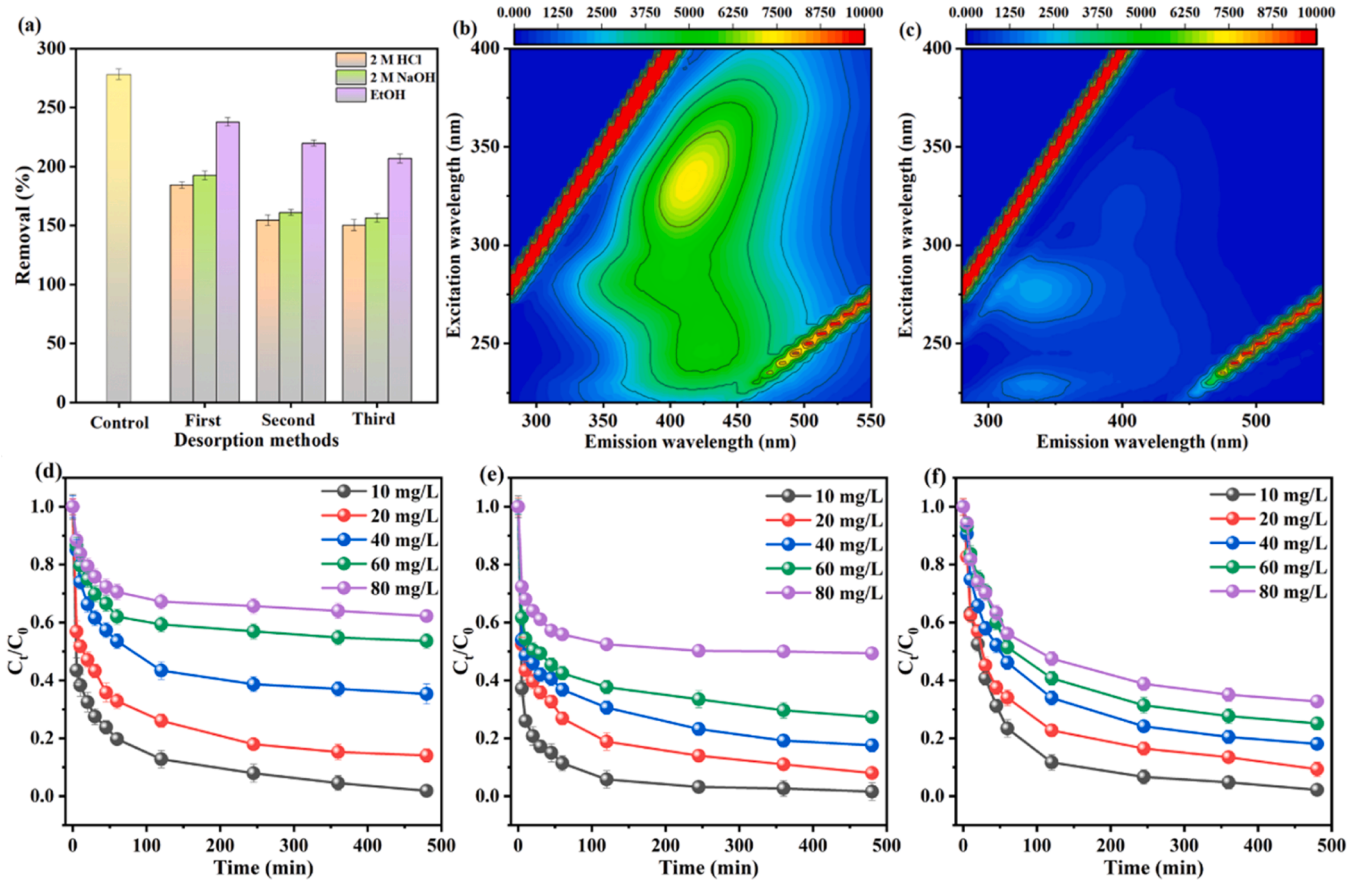

Fig. 8. (a) Three cycles of adsorption-desorption tests were conducted on PCH using various desorption approaches. 3D EEMs of actual wastewater (a) before and (b) after adsorption by PCH. Adsorption performances of PCH on (d) OG, (e) TC, and (f) AP. (C_0 =10–80 mg/L, adsorbent dosage =0.1 g/L, the reaction time =6 h, pH=6, at 25∘C).

CRediT authorship contribution statement

Ke-Qing Du: Writing – original draft, Visualization, Methodology, Investigation, Data curation, Conceptualization. **Jun-Feng Li:** Supervision, Resources, Methodology. **Muhammad Arsalan Farid:** Writing – review & editing. **Wen-Huai Wang:** Writing – review & editing, Funding acquisition. **Guang Yang:** Investigation, Funding acquisition, Formal analysis.

Declaration of Competing Interest

The authors declare that they have no known competing financial interests or personal relationships that could have appeared to influence the work reported in this paper.

Acknowledgments

The authors wish to express the great appreciation of the financial support from the National Natural Science Foundation of China (52269006); Projects of Xinjiang Production and Construction Corps (2022BC001, 2022DB023, 2023AB059, 2023TSYCCX0114); Project of Shihezi (2023NY01) and The Third Xinjiang Scientific Expedition Program (2021xjkk0804); Project of Shihezi University (KX00860201); Project of National Natural Science Foundation of China (52300214); Project of Annual Youth Doctoral Program of Xinjiang Uyghur Autonomous Region 'Tianchi Elite' Introduction Plan (CZ002305).

Appendix A. Supporting information

Supplementary data associated with this article can be found in the online version at doi:10.1016/j.indcrop.2025.120649.

Data availability

Data will be made available on request.

References

Afzal, M.Z., Yue, R., Sun, X.-F., Song, C., Wang, S.-G., 2019. Enhanced removal of ciprofloxacin using humic acid modified hydrogel beads. J. Colloid Interface Sci. 543, 76–83. https://doi.org/10.1016/j.jcis.2019.01.083.

Akhavan, O., 2015. Bacteriorhodopsin as a superior substitute for hydrazine in chemical reduction of single-layer graphene oxide sheets. Carbon 81, 158–166. https://doi.org/10.1016/j.carbon.2014.09.044.

Akter, S., Islam, M.S., Kabir, M.H., Shaikh, M.A.A., Gafur, M.A., 2022. UV/TiO_2 photodegradation of metronidazole, ciprofloxacin and sulfamethoxazole in aqueous solution: An optimization and kinetic study. Arab. J. Chem. 15 (7), 103900. https://doi.org/10.1016/j.arabjc.2022.103900.

Alver, E., Metin, A.Ü., Brouers, F., 2020. Methylene blue adsorption on magnetic alginate/rice husk bio-composite. Int. J. Biol. Macromol. 154, 104–113. https://doi.org/10.1016/j.ijbiomac.2020.02.330.

Angin, D., 2013. Effect of pyrolysis temperature and heating rate on biochar obtained from pyrolysis of safflower seed press cake. Bioresour. Technol. 128, 593–597. https://doi.org/10.1016/j.biortech.2012.10.150.

Azzam, A.B., Tokhy, Y.A., El Dars, F.M., Younes, A.A., 2022. Construction of porous biochar decorated with NiS for the removal of ciprofloxacin antibiotic from pharmaceutical wastewaters. J. Water Process. Eng. 49, 103006. https://doi.org/10.1016/j.jwpe.2022.103006.

Bello, O.S., Adegoke, K.A., Sarumi, O.O., Lameed, O.S., 2019. Functionalized locust bean pod (Parkia biglobosa) activated carbon for Rhodamine B dye removal. Heliyon 5 (8), e02323. https://doi.org/10.1016/j.heliyon.2019.e02323.

Carabineiro, S.A., Thavorn-Amornsri, T., Pereira, M.F., Figueiredo, J.L., 2011. Adsorption of ciprofloxacin on surface-modified carbon materials. Water Res 45, 4583–4591. https://doi.org/10.1016/j.watres.2011.06.008.

Che, H., Wei, G., Fan, Z., Zhu, Y., Zhang, L., Wei, Z., Huang, X., Wei, L., 2023. Super facile one-step synthesis of sugarcane bagasse derived N-doped porous biochar for adsorption of ciprofloxacin. J. Environ. Manag. 335, 117566. https://doi.org/10.1016/j.jenvman.2023.117566.

Chen, C., Yang, F., Beesley, L., Trakal, L., Ma, Y., Sun, Y., Zhang, Z., Ding, Y., 2022. Removal of cadmium in aqueous solutions using a ball milling–assisted one-pot pyrolyzed iron-biochar composite derived from cotton husk. Environ. Sci. Pollut. R. 30 (5), 12571–12583. https://doi.org/10.1007/s11356-022-22828-w.

Cheng, Y., Wang, B., Shen, J., Yan, P., Kang, J., Wang, W., Bi, L., Zhu, X., Li, Y., Wang, S., Shen, L., Chen, Z., 2022. Preparation of novel N-doped biochar and its high adsorption capacity for atrazine based on π–π electron donor-acceptor interaction. J. Hazard. Mater. 432, 128757. https://doi.org/10.1016/j.jhazmat.2022.128757.

Deng, Z., Zhu, J., Li, P., Du, Z., Qi, X., Chen, X., Mu, R., Zeng, C., Ma, Y., Zhang, Z., 2023. Effective adsorptive removal of tetracycline from aqueous solution by Zn-BTC@SBC derived from sludge:Experimental study and density functional theory (DFT) calculations. J. Mol. Liq. 384, 122283. https://doi.org/10.1016/j.molliq.2023.122283.

Ding, D.H., Yang, S.J., Qian, X.Y., Chen, L.W., Cai, T.M., 2020a. Nitrogen-doping positively whilst sulfur-doping negatively affect the catalytic activity of biochar for the degradation of organic contaminant. Appl. Catal. B-Environ. Energy 263, 118348. https://doi.org/10.1016/j.apcatb.2019.118348.

Ding, D.H., Zhou, L., Kang, F.X., Yang, S.J., Chen, R.Z., Cai, T.M., Duan, X.G., Wang, S.B., 2020b. Synergistic adsorption and oxidation of ciprofloxacin by biochar derived from metal-enriched phytoremediation plants: experimental and computational insights. ACS Appl. Mater. Interfaces 12 (48), 53788–53798. https://doi.org/10.1021/acsami.0c15861.

Fries, E., Crouzet, C., Michel, C., Togola, A., 2016. Interactions of ciprofloxacin (CIP), titanium dioxide (TiO2) nanoparticles and natural organic matter (NOM) in aqueous suspensions. Sci. Total Environ. 564, 971–976. https://doi.org/10.1016/j.scitotenv.2015.12.023.

Gani, K., Kazmi, A., Asce, M., Asce, S., 2017. Contamination of emerging contaminants in indian aquatic sources: first overview of the situation. J. Hazard. 21, 1–12. https://doi.org/10.1061/(ASCE)HZ.2153-5515.0000348.

Ghasemi, J., Asadpour, S., 2007. Thermodynamics' study of the adsorption process of methylene blue on activated carbon at different ionic strengths. J. Chem. Thermodyn. 39, 967–971. https://doi.org/10.1016/j.jct.2006.10.018.

Guo, Y., Rockstraw, D.A., 2007. Physicochemical properties of carbons prepared from pecan shell by phosphoric acid activation. Bioresour. Technol. 98, 1513–1521. https://doi.org/10.1016/j.biortech.2006.06.027.

Hamadeen, H.M., Elkhatib, E.A., 2022. New nanostructured activated biochar for effective removal of antibiotic ciprofloxacin from wastewater: adsorption dynamics and mechanisms. Environ. Res. 210, 112929. https://doi.org/10.1016/j.envres.2022.112929.

Hu, Y., Zhu, Y., Zhang, Y., Lin, T., Zeng, G., Zhang, S., 2019. An efficient adsorbent: Simultaneous activated and magnetic ZnO doped biochar derived from camphor leaves for ciprofloxacin adsorption. Bioresour. Technol. 288, 121511. https://doi.org/10.1016/j.biortech.2019.121511.

Islam, M.S., Kwak, J.-H., Nzediegwu, C., Wang, S., Palansuriya, K., Kwon, E.E., Naeth, M. A., El-Din, M.G., Ok, Y.S., Chang, S.X., 2021. Biochar heavy metal removal in aqueous solution depends on feedstock type and pyrolysis purging gas. Environ. Pollut. 281, 117094. https://doi.org/10.1016/j.envpol.2021.117094.

Jiang, H., Li, X., Dai, Y., 2023. Phosphoric acid activation of cow dung biochar for adsorbing enrofloxacin in water: Icing on the cake. Environ. Pollut. 341, 122887. https://doi.org/10.1016/j.envpol.2023.122887.

Jiang, Y., Ran, J.B., Mao, K., Yang, X.F., Zhong, L., Yang, C.Y., Feng, X.B., Zhang, H., 2022. Recent progress in Fenton/Fenton-like reactions for the removal of antibiotics in aqueous environments. Ecotoxicol. Environ. Saf. 236, 114364. https://doi.org/10.1016/j.ecoenv.2022.113464.

Kang, S.M., Xiao, L.P., Meng, L.Y., Zhang, X.M., Sun, R.C., 2012. Isolation and structural characterization of lignin from cotton stalk treated in an ammonia hydrothermal system. Int. J. Mol. Sci. 13 (11), 15209–15226. https://doi.org/10.3390/ijms131115209.

Khan, M.H., Akash, N.M., Akter, S., Rukh, M., Nzediegwu, C., Islam, M.S., 2023. A comprehensive review of coconut-based porous materials for wastewater treatment and CO_2 capture. J. Environ. Manag. 338, 117825. https://doi.org/10.1016/j.jenvman.2023.117825.

Khanday, W.A., Ahmed, M.J., Okoye, P.U., Hummadi, E.H., Hameed, B.H., 2019. Single-step pyrolysis of phosphoric acid-activated chitin for efficient adsorption of cephalexin antibiotic. Bioresour. Technol. 280, 255–259. https://doi.org/10.1016/j.biortech.2019.02.003.

Kunwar, B., Pittman, C.U., Mohan, D., Mlsna, T., 2015. Sorptive removal of salicylic acid and ibuprofen from aqueous solutions using pine wood fast pyrolysis biochar. Chem. Eng. J. 265, 219–227. https://doi.org/10.1016/j.cej.2014.12.006.

Kwak, J.-H., Islam, M.S., Wang, S., Messele, S.A., Naeth, M.A., El-Din, M.G., Chang, S.X., 2019. Biochar properties and lead(II) adsorption capacity depend on feedstock type, pyrolysis temperature, and steam activation. Chemosphere 231, 393–404. https://doi.org/10.1016/j.chemosphere.2019.05.128.

Lapworth, D.J., Baran, N., Stuart, M.E., Ward, R.S., 2012. Emerging organic contaminants in groundwater: a review of sources, fate and occurrence. Environ. Pollut. 163, 287–303. https://doi.org/10.1016/j.envpol.2011.12.034.

Li, H., Zhang, D., Han, X., Xing, B., 2014. Adsorption of antibiotic ciprofloxacin on carbon nanotubes: pH dependence and thermodynamics. Chemosphere 95, 150–155. https://doi.org/10.1016/j.chemosphere.2013.08.053.

Li, J., Yu, G., Pan, L., Li, C., You, F., Xie, S., Wang, Y., Ma, J., Shang, X., 2018. Study of ciprofloxacin removal by biochar obtained from used tea leaves. J. Environ. Sci. 73, 20–30. https://doi.org/10.3389/fenvs.2024.1353267.

Li, J., Yu, G., Pan, L., Li, C., You, F., Wang, Y., 2022. Ciprofloxacin adsorption by biochar derived from co-pyrolysis of sewage sludge and bamboo waste. Environ. Sci. Pollut. R. 287, 131962. https://doi.org/10.1007/s11356-020-08333-y.

Li, N., Yin, M., Tsang, D.C.W., Yang, S., Wang, J., 2019. Mechanisms of U(VI) removal by biochar derived from Ficus microcarpa aerial root: a comparison between raw and modified biochar. Sci. Total Environ. 697, 134115. https://doi.org/10.1016/j.scitotenv.2019.134115.

Liu, Q., Li, D.M., Cheng, H.R., Cheng, J.H., Du, K.S., Hu, Y.Y., Chen, Y.C., 2021. High mesoporosity phosphorus-containing biochar fabricated from Camellia oleifera shells: Impressive tetracycline adsorption performance and promotion of pyrophosphate-like surface functional groups (C-O-P bond). Bioresour. Technol. 329, 124922. https://doi.org/10.1016/j.biortech.2021.124922.

Lu, P., Lin, K., Gan, J., 2020. Enhanced ozonation of ciprofloxacin in the presence of bromide: kinetics, products, pathways, and toxicity. Water Res 183, 116105. https://doi.org/10.1016/j.watres.2020.116105.

Martínez-Alvarenga, H., Gutiérrez, M.C., Gomez-Cámer, J.L., Benítez, A., Martín, M.A., Caballero, A., 2024. Integral evaluation of effective conversion of sewage sludge from WWTP into highly porous activated carbon. J. Environ. Manag. 351, 119822. https://doi.org/10.1016/j.jenvman.2023.119822.

Migliore, L., Cozzolino, S., Fiori, M., 2000. Phytotoxicity to and uptake of flumequine used in intensive aquaculture on the aquatic weed, Lythrum salicaria L. Chemosphere 40, 741–750. https://doi.org/10.1016/S0045-6535(99)00448-8.

Ng, C., Marshall, W.E., Rao, R.M., Bansode, R.R., Losso, J.N., 2003. Activated carbon from pecan shell: process description and economic analysis. Ind. Crop Prod. 17, 209–217. https://doi.org/10.1016/S0926-6690(03)00002-5.

Nguyen, T.-B., Truong, Q.-M., Chen, C.-W., Doong, R.-a, Chen, W.-H., Dong, C.-D., 2022. Mesoporous and adsorption behavior of algal biochar prepared via sequential hydrothermal carbonization and $ZnCl_2$ activation. Bioresour. Technol. 346, 126351. https://doi.org/10.1016/j.biortech.2021.126351.

Nguyen, T.K.T., Nguyen, T.B., Chen, W.H., Chen, C.W., Patel, A.K., Bui, X.T., Chen, L.J., Singhania, R.R., Dong, C.D., 2023. Phosphoric acid-activated biochar derived from sunflower seed husk: selective antibiotic adsorption behavior and mechanism. Bioresour. Technol. 371, 128593. https://doi.org/10.1016/j.biortech.2023.128593.

Oliveira, M.G., Spaolonzi, M.P., Duarte, E.D.V., Costa, H.P.S., Silva, M.G.C., Vieira, M.G. A., 2023. Adsorption kinetics of ciprofloxacin and ofloxacin by green-modified carbon. Environ. Res 233, 116503. https://doi.org/10.1007/s11356-024-33252-7.

Penafiel, M.E., Matesanz, J.M., Vanegas, E., Bermejo, D., Mosteo, R., Ormad, M.P., 2021. Comparative adsorption of ciprofloxacin on sugarcane bagasse from Ecuador and on commercial powdered activated carbon. Sci. Total Environ. 750, 141498. https://doi.org/10.1016/j.scitotenv.2022.154309.

Peng, H., Gao, P., Chu, G., Pan, B., Peng, J., Xing, B., 2017. Enhanced adsorption of Cu(II) and Cd(II) by phosphoric acid-modified biochars. Environ. Pollut. 229, 846–853. https://doi.org/10.1016/j.envpol.2017.07.004.

Qiao, M., Ying, G.G., Singer, A.C., Zhu, Y.G., 2018. Review of antibiotic resistance in China and its environment. Environ. Int. 110, 160–172. https://doi.org/10.1016/j.envint.2017.10.016.

Qu, J., Wang, Y., Tian, X., Jiang, Z., Deng, F., Tao, Y., Jiang, Q., Wang, L., Zhang, Y., 2020. KOH-activated porous biochar with high specific surface area for adsorptive removal of chromium (VI) and naphthalene from water: affecting factors, mechanisms and reusability exploration J. Hazard. Mater 401. https://doi.org/10.1016/j.jhazmat.2020.123292.

Roy, H., Prantika, T.R., Riyad, M.H., Paul, S., Islam, M.S., 2022b. Synthesis, characterizations, and RSM analysis of Citrus macroptera peel derived biochar for textile dye treatment. South Afr. J. Chem. Eng. 41, 129–139. https://doi.org/10.1016/j.sajce.2022.05.008.

Roy, H., Islam, M.S., Arifin, M.T., Firoz, S.H., 2022a. Chitosan-ZnO decorated Moringa oleifera seed biochar for sequestration of methylene blue: isotherms, kinetics, and response surface analysis. Environ. Nanotechnol., Monit. Manag. 18, 100752. https://doi.org/10.1016/j.enmm.2022.100752.

SEPA, 2008. Discharge standard of water pollutants for pharmaceutical industry Chemical synthesis products category (GB21904-2008). Beijing.

Septian, A., Shin, W.S., 2020. Removal of sulfadiazine and ciprofloxacin by clays and manganese oxides: coupled sorption-oxidation kinetic model. Chemosphere 250, 126251. https://doi.org/10.1016/j.chemosphere.2020.126251.

Shen, R., Yu, Y., Lan, R., Yu, R., Yuan, Z., Xia, Z., 2019. The cardiovascular toxicity induced by high doses of gatifloxacin and ciprofloxacin in zebrafish. Environ. Pollut. 254, 112861. https://doi.org/10.1016/j.envpol.2019.07.029.

Sun, Y., Li, H., Li, G., Gao, B., Yue, Q., Li, X., 2016. Characterization and ciprofloxacin adsorption properties of activated carbons prepared from biomass wastes by H_3PO_4 activation. Bioresour. Technol. 217, 239–244. https://doi.org/10.1016/j.biortech.2016.03.047.

Wang, B., Jiang, Y., Li, F., Yang, D., 2017. Preparation of biochar by simultaneous carbonization, magnetization and activation for norfloxacin removal in water. Bioresour. Technol. 233, 159–165. https://doi.org/10.1016/j.biortech.2017.02.103.

Wang, S., Liu, Y., Song, X., Wei, S., Li, J., Nie, J., Qin, D., Sun, X., 2016. Effects of cotton straw returning on soil organic carbon, nitrogen, phosphorus and potas-sium contents in soil aggregates. Ying Yong Sheng Tai Xue Bao 27, 3944–3952. https://doi.org/10.13287/j.1001 - 9332.201612.015.

Wei, H., Deng, S., Huang, Q., Nie, Y., Wang, B., Huang, J., Yu, G., 2013. Regenerable granular carbon nanotubes/alumina hybrid adsorbents for diclofenac sodium and carbamazepine removal from aqueous solution. Water Res 47, 4139–4147. https://doi.org/10.1016/j.watres.2012.11.062.

Xue, Y.T., Guo, Y.T., Zhang, X., Kamali, M., Aminabhavi, T.M., Appels, L., Dewil, R., 2022. Efficient adsorptive removal of ciprofloxacin and carbamazepine using modified pinewood biochar-A kinetic, mechanistic study. Chem. Eng. J. 450, 137896. https://doi.org/10.1016/j.cej.2022.137896.

Yahiat, S., Fourcade, F., Brosillon, S., Amrane, A., 2011. Removal of antibiotics by an integrated process coupling photocatalysis and biological treatment - case of tetracycline and tylosin. Int. Biodeter. Bioderg. 65, 997–1003. https://doi.org/10.1016/j.ibiod.2011.07.009.

Zhang, H., Quan, H., Yin, S., Sun, L., Lu, H., 2022. Unraveling the toxicity associated with ciprofloxacin biodegradation in biological wastewater treatment. Environ. Sci. Technol. 56, 15941–15952. https://doi.org/10.1021/acs.est.2c04387.

Zhang, P., Zhang, X., Yuan, X., Xie, R., Han, L., 2021. Characteristics, adsorption behaviors, Cu(II) adsorption mechanisms by cow manure. Bioresour. Technol. 331, 125013. https://doi.org/10.1016/j.biortech.2021.125013.

Zhang, T., Li, T., Zhou, Z., Li, Z., Zhang, S., Wang, G., Xu, X., Pu, Y., Jia, Y., Liu, X., Li, Y., 2023. Cadmium-resistant phosphate-solubilizing bacteria immobilized on phosphoric acid-ball milling modified biochar enhances soil cadmium passivation and phosphorus bioavailability. Sci. Total Environ. 877, 162812. https://doi.org/10.1016/j.scitotenv.2023.162812.

Zhang, Z.L., Li, Y., Zong, Y.M., Yu, J., Ding, H., Kong, Y.L., Ma, J.Y., Ding, L., 2022. Efficient removal of cadmium by salts modified-biochar: performance assessment, theoretical calculation, and quantitative mechanism analysis. Bioresour. Technol. 361, 127717. https://doi.org/10.1016/j.biortech.2022.127717.

Zhou, Y., He, Y., He, Y., Liu, X., Xu, B., Yu, J., Dai, C., Huang, A., Pang, Y., Luo, L., 2018. Analyses of tetracycline adsorption on alkali-acid modified magnetic biochar: site energy distribution consideration. Sci. Total Environ. 650, 2260–2266. https://doi.org/10.1016/j.scitotenv.2018.09.393.

Zhou, Y., Li, F., Xin, Q., Li, Y., Lin, Z., 2024. Historical variability of cotton yield and response to climate and agronomic management in Xinjiang, China. Sci. Total Environ. 912, 169327. https://doi.org/10.1016/j.scitotenv.2023.169327.